EUROPEAN UROLOGY 65 (2014) 947–964

available at www.sciencedirect.com
journal homepage: www.europeanurology.com

European Association of Urology

Platinum Priority – Review – Endo-urology

Editorial by M. Pilar Laguna on pp. 965–966 of this issue

Current Perspectives in the Use of Molecular Imaging To Target Surgical Treatments for Genitourinary Cancers

Francesco Greco [a,*], *Jeffrey A. Cadeddu* [b], *Inderbir S. Gill* [c], *Jihad H. Kaouk* [d], *Mesut Remzi* [e], *R. Houston Thompson* [f], *Fijs W.B. van Leeuwen* [g], *Henk G. van der Poel* [h], *Paolo Fornara* [a], *Jens Rassweiler* [i]

[a] *Department of Urology and Renal Transplantation, Martin-Luther University, Halle an der Saale, Germany;* [b] *Department of Urology, University of Texas Southwestern Medical Center, Dallas, TX, USA;* [c] *USC Institute of Urology, Catherine and Joseph Aresty Department of Urology, Keck School of Medicine, University of Southern California, Los Angeles, CA, USA;* [d] *Glickman Urological & Kidney Institute, Cleveland Clinic, Cleveland, OH, USA;* [e] *Department of Urology, Landesklinikum Korneuburg, Korneuburg, Austria;* [f] *Department of Urology, Mayo Clinic, Rochester, MN, USA;* [g] *Department of Radiology, Interventional Molecular Imaging Laboratory, Leiden University Medical Center, Leiden, The Netherlands;* [h] *Department of Urology, Netherlands Cancer Institute-Antoni van Leeuwenhoek Hospital, Amsterdam, The Netherlands;* [i] *Department of Urology, SLK Kliniken Heilbronn, University of Heidelberg, Heilbronn, Germany*

Article info

Article history:
Accepted July 17, 2013
Published online ahead of print on August 7, 2013

Keywords:
Molecular imaging
Genitourinary oncologic surgery
Surgical navigation
Image-guided surgery
Augmented reality

Abstract

Context: Molecular imaging (MI) entails the visualisation, characterisation, and measurement of biologic processes at the molecular and cellular levels in humans and other living systems. Translating this technology to interventions in real-time enables interventional MI/image-guided surgery, for example, by providing better detection of tumours and their dimensions.
Objective: To summarise and critically analyse the available evidence on image-guided surgery for genitourinary (GU) oncologic diseases.
Evidence acquisition: A comprehensive literature review was performed using PubMed and the Thomson Reuters Web of Science. In the free-text protocol, the following terms were applied: *molecular imaging, genitourinary oncologic surgery, surgical navigation, image-guided surgery*, and *augmented reality*. Review articles, editorials, commentaries, and letters to the editor were included if deemed to contain relevant information. We selected 79 articles according to the search strategy based on the Preferred Reporting Items for Systematic Reviews and Meta-analysis criteria and the IDEAL method.
Evidence synthesis: MI techniques included optical imaging and fluorescent techniques, the augmented reality (AR) navigation system, magnetic resonance imaging spectroscopy, positron emission tomography, and single-photon emission computed tomography. Experimental studies on the AR navigation system were restricted to the detection and therapy of adrenal and renal malignancies and in the relatively infrequent cases of prostate cancer, whereas fluorescence techniques and optical imaging presented a wide application of intraoperative GU oncologic surgery. In most cases, image-guided surgery was shown to improve the surgical resectability of tumours.
Conclusions: Based on the evidence to date, image-guided surgery has promise in the near future for multiple GU malignancies. Further optimisation of targeted imaging agents, along with the integration of imaging modalities, is necessary to further enhance intraoperative GU oncologic surgery.

* Corresponding author. Department of Urology and Kidney Transplantation, Martin-Luther-University, Ernst-Grube-Strasse 40, 06120 Halle an der Saale, Germany.
E-mail address: francesco.greco@uk-halle.de (F. Greco).

0302-2838/$ – see back matter
http://dx.doi.org/10.1016/j.eururo.2013.07.033

1. Introduction

In recent decades, imaging technologies have realized significant developments, resulting in their current important role in clinical oncology [1]. The field has expanded greatly and now comprises various modalities including ultrasonography (US), computed tomography (CT), magnetic resonance imaging (MRI), positron emission tomography (PET), and single-photon emission computed tomography (SPECT) [2–4]. Because each modality has its specific advantages and disadvantages, combining different techniques (eg, PET and CT) has become the practice for tumour detection, staging, and treatment evaluation [1–5]. However, when surgery is required, translation of these molecular images to the operative field remains a challenging obstacle.

Recently, advances in molecular imaging (MI) technology enable the noninvasive imaging of specific molecular pathways that are fundamentally involved in disease processes [6–8].Various hallmarks of cancer can be used to detect malignant cells or tissues such as growth factor signalling receptors, limitless replicative potential, sustained angiogenesis, and increased proteolytic activity resulting in tissue invasion and metastasis [9,10]. MI evaluates the molecular signature and changes in cellular physiology and function rather than anatomy. These molecular pathways are likely to be expressed earlier than anatomic deformation, allowing more sensitive representations of the disease process. In addition, detecting tumours via their unique molecular signatures may help to significantly improve the specificity of diagnoses. Ideally this information is put in the hands of the surgeon in real-time to warrant image-guided surgery.

This review summarises and critically analyses the currently available evidence of intraoperative navigation and imaged-guided surgery for genitourinary (GU) oncologic surgery.

2. Evidence acquisition

A comprehensive literature review was performed using PubMed and Thomson Reuters Web of Science between April 1995 and April 2013. Using free-text protocol, the following terms were applied: *molecular imaging, genitourinary oncologic surgery, surgical navigation, image-guided surgery*, and *augmented reality*. Review articles, editorials, commentaries, and letters to the editor were included only if deemed to contain relevant information. Cited references from the selected articles and from review articles retrieved in the search were also assessed for significant manuscripts not previously included. Studies published only as an abstract or presented without an abstract, and reports from meetings and studies not published in English were not included in the review.

We selected 79 articles according to the search strategy based on the Preferred Reporting Items for Systematic Reviews and Meta-analysis (PRISMA) criteria [11] (Fig. 1; Table 1).

To describe and assess the development of each surgical innovation and at the same time to clearly depict the stages of the research, all included studies were also segmented into sequential stages according to the IDEAL methodology (I = idea, D = development, E = exploration, A = assessment, L = long-term study) [12].

3. Evidence synthesis

3.1. Quality of the studies and level of evidence

According to the IDEAL methodology [12], 15 studies represented stage 0 [1,7,8,16,17,19,30,35,36,48–50,62,68,72], 11 studies were classified as stage 1 [23,25,28,31,32,51,54,57–60], 18 studies as stage 2a [24,26,27,37,41,43,45,52,61,63–65,67,70,81,83,84], 20 studies as stage 2b [2,3,5,6,9,10,15,22,33,34,44,46,47,66,69,71,78–80], 11 studies as stage 3 [4,18,20,29,38–40,42,53,55,75], and 5 studies were considered stage 4 [21,73,74,76,77].

We defined clinical studies included in the analysis according to the levels of evidence defined by the Oxford Centre for Evidence-based Medicine (http://www.cebm.net). There was one study with level of evidence (LE) 1a [82], 21 studies with LE 1b [17,23,25,33,35,39,42,46,48,49,52,53,60,61,63,64,75–79], 26 studies with LE 2a [1–7,9,10,15,16,18–22,24,29,30,35,43–45,71,73,74], 19 studies with LE 2b [8,26–28,32,36,41,51,54,55,57–59,62,67–69,72,80], 10 studies with LE 3b [37,38,40,47,50,65,66,70,81,83], and 2 studies with LE 4 [31,84].

3.2. Interventional molecular imaging

3.2.1. Definition

A number of definitions have been proposed for MI. In 2005, an MI summit, sponsored by the Radiological Society of North America and the Society of Nuclear Medicine and Molecular Imaging (SNM), recommended the following definition: "Molecular imaging techniques directly or indirectly monitor and record the spatiotemporal distribution of molecular or cellular processes for biochemical, biologic, diagnostic, or therapeutic applications" [13].

In 2007, the SNM Molecular Imaging Centre of Excellence recommended an expanded definition, whereby MI represents the visualisation, characterisation, and measurement of biologic processes at the molecular and cellular levels in humans and other living systems. MI typically consists of two-dimensional (2D) or three-dimensional (3D) imaging as well as quantification over time.

The techniques used to enable an interventional MI/image-guided surgery include optical imaging and fluorescent techniques, an augmented reality (AR) navigation system, MRI spectroscopy, PET, and SPECT [14]. Interventional MI has the potential to personalise patient care because it can reveal the clinical biology of the patient and of the tumour [6].

3.2.2. Techniques and new developments

Major strides in our understanding of the molecular biology of GU malignancies have led to the development of novel techniques in biomedical imaging [15]. In GU oncologic surgery, intraoperative assessment of the tumour-free margin is critical for the prognosis of the patient. Currently,

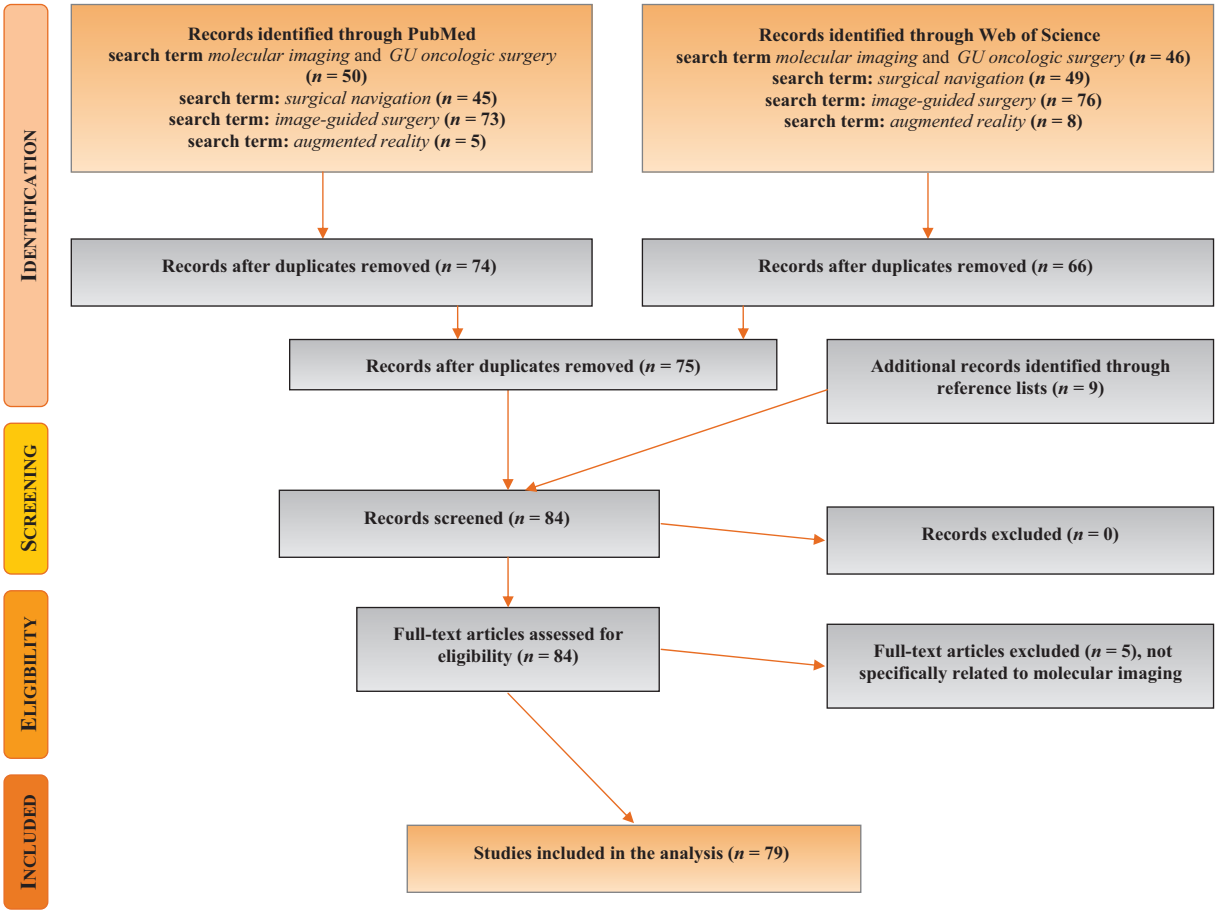

Fig. 1 – Preferred Reporting Items for Systematic Reviews and Meta-analysis flow diagram. GU = genitourinary.

surgeons rely on the visual appearance and digital palpation of the tumour.

3.2.2.1. Optical imaging. Optical imaging techniques have the potential to provide real-time visualisation of the tumour during its surgical resection (Table 2). In optical imaging, properties of light emitted from a light source are exploited to image anatomic or chemical characteristics of tissue. Optical imaging can be performed using either the properties intrinsic to the tissue or, analogous to many radiolabelled agents, using ligands conjugated to an optically active antenna to target a recognised disease biomarker [1]. In this way, optical imaging could provide a valuable addition to the current modalities of image-guided surgery [8].

Conventional fluorescent techniques use probes in the visible light spectrum (approximately 400–750 nm), which is not optimal for intraoperative identification. Over the last decade, the development of near-infrared fluorescence (NIRF) cameras that are able to visualise fluorophores and nanomaterials has led to a revolution in optical imaging [16–19].

This combination provides an increasing tissue penetration and allows more precise localisation of cancer. But it should be noted that signal penetration of this technology remains confined below 1 cm [16–19]. Thus the properties of near-infrared (NIR) optical imaging are suited for real-time visualisation of (superficial) lesions. Ultimately, intraoperative visualisation of tumour margins may improve radical resection without unnecessary damage to healthy tissue.

Photodynamic diagnosis (PDD) for cystoscopy represents an optical technique using fluorescence as a contrast mechanism to indicate pathologic tissue. It is based on the phenomenon of concentrations of fluorescent molecules differing in normal and pathologic tissue. Absorption of light of the appropriate wavelength excites the electro-vibrational state of fluorophore molecules. When these molecules relax to ground state, a photon is emitted to account for the energy difference. The fluorescent photon has less energy than the excitation photon; because the energy of light is inversely proportional to its wavelength, the emitted light has a longer wavelength than the illuminating light. Therefore, discrimination between the two types of light is possible [20].

PDD can be based on either the presence of natural fluorescent molecules (endogenous or autofluorescence) or the administration of agents that increase the production of fluorescent molecules (exogenous fluorescence). Several commercially available agents have been used to induce exogenous fluorescence, but presently hypericin, 5-aminolaevulinic acid (5-ALA), and its ester hexaminolevulinate are applied most often.

Table 1 – PRISMA checklist of items to include when reporting a systematic review [11]

Section/Topic	Item no.	Checklist item
TITLE		
Title	1	Identify the report as a systematic review, meta-analysis, or both.
ABSTRACT	2	Provide a structured summary including, as applicable, background; objectives; data sources; study eligibility criteria, participants, and interventions; study appraisal and synthesis methods; results; limitations; conclusions and implications of key findings; systematic review registration number.
Structured summary		
INTRODUCTION		
Rationale	3	Describe the rationale for the review in the context of what is already known.
Objectives	4	Provide an explicit statement of questions being addressed with reference to participants, interventions, comparisons, outcomes, and study design (PICOS).
METHODS		
Protocol and registration	5	Indicate if a review protocol exists, if and where it can be accessed (eg, Web address), and, if available, provide registration information including registration number.
Eligibility criteria		
Information sources	6	Specify study characteristics (eg, PICOS, length of follow-up) and report characteristics (eg, years considered, language, publication status) used as criteria for eligibility, giving rationale.
Search		
Study selection	7	Describe all information sources (eg, databases with dates of coverage, contact with study authors to identify additional studies) in the search and date last searched.
Data collection process		
Data items	8	Present full electronic search strategy for at least one database, including any limits used, such that it could be repeated.
Risk of bias in individual studies		
Summary measures	9	State the process for selecting studies (ie, screening, eligibility, included in systematic review, and, if applicable, included in the meta-analysis).
Synthesis of results		
Risk of bias across studies	10	Describe method of data extraction from reports (eg, piloted forms, independently, in duplicate) and any processes for obtaining and confirming data from investigators.
Additional analyses		
	11	List and define all variables for which data were sought (eg, PICOS, funding sources) and any assumptions and simplifications made.
	12	Describe methods used for assessing risk of bias of individual studies (including specification of whether this was done at the study or outcome level), and how this information is to be used in any data synthesis.
	13	State the principal summary measures (eg, risk ratio, difference in means).
	14	Describe the methods of handling data and combining results of studies, if done, including measures of consistency (eg, I2) for each meta-analysis.
	15	Specify any assessment of risk of bias that may affect the cumulative evidence (eg, publication bias, selective reporting within studies).
	16	Describe methods of additional analyses (eg, sensitivity or subgroup analyses, meta-regression), if done, indicating which were prespecified.
RESULTS		
Study selection	17	Give numbers of studies screened, assessed for eligibility, and included in the review, with reasons for exclusions at each stage, ideally with a flow diagram.
Study characteristics		
Risk of bias within studies	18	For each study, present characteristics for which data were extracted (eg, study size, PICOS, follow-up period) and provide the citations.
Results of individual studies		
Synthesis of results	19	Present data on risk of bias of each study and, if available, any outcome-level assessment (see item 12).
Risk of bias across studies	20	For all outcomes considered (benefits or harms), present, for each study: (a) simple summary data for each intervention group and (b) effect estimates and confidence intervals, ideally with a forest plot.
Additional analysis		
	21	Present results of each meta-analysis done, including confidence intervals and measures of consistency.
	22	Present results of any assessment of risk of bias across studies (see item 15).
	23	Give results of additional analyses, if done (eg, sensitivity or subgroup analyses, meta-regression [see item 16]).
DISCUSSION		
Summary of evidence	24	Summarise the main findings including the strength of evidence for each main outcome; consider their relevance to key groups (eg, health care providers, users, and policymakers).
Limitations		
Conclusions	25	Discuss limitations at study and outcome level (eg, risk of bias), and at review level (eg, incomplete retrieval of identified research, reporting bias).
	26	Provide a general interpretation of the results in the context of other evidence, and implications for future research.
FUNDING		
Funding	27	Describe sources of funding for the systematic review and other support (eg, supply of data); role of funders for the systematic review.

Endoscopes with specially developed light sources and filters (yellow) are used. A foot pedal or push button on the camera enables the switch from white-light cystoscopy (WLC) to PDD mode. By illuminating the bladder wall with blue light, the malignant tissue appears intensely pink or red on a blue background [21].

3.2.2.2. Image-fusion technologies. Current MI techniques such as PET are being used to evaluate patients for soft tissue metastases, particularly for prostate, renal, testicular, and bladder malignancies, in oncology centres and could serve as a guide for ablative therapy (Table 3) [15,22]. Lastly, immune PET with anhydrase-IX antibodies may be able to detect residual or recurrent clear cell kidney cancers after focal ablative therapy [23].

Image-fusion technologies and image-augmented navigation have been developed in several other fields and have tremendous potential for medical applications. These

Table 2 – Application of optical imaging to genitourinary tumours

GU tumour type	Molecular imaging	Stage of research
Prostate cancer	TRUS with Doppler	- Decreases PSM - Increases tumour stage prediction - Small not randomised studies available
	Fluorescence (FG, FB, FR, GFPRv)	- Improves identification of NVBs - Only animal trials
	PDD (PpIX)	- Decreases PSM - Easier and less time consuming - Higher rate of false negatives in the open cases versus endoscopic cases
	ICG-99mTc-NanoColl	- Improves the surgical accuracy of laparoscopic LN dissection
Renal cancer	NIRF with ICG	- Maximises oncologic control - Decreases PSM - Small not randomised studies available
	PDD (5-ALA)	- Decreases PSM - Better visualisation of the tumour - Accuracy of 94% - Small not randomised studies available
	HSI technique	- Decreases WIT - Decreases postoperative renal damage - Increases tissue oxygenation - In experimental phase (humans)
	RVS	- Reduces the difficulty of interpretation of the lower-resolution ultrasound image - Achieves a better understanding of the pre-nephrectic anatomy - Helps to understand the hidden anatomy beneath the US interface - In experimental phase (humans)
Testicular cancer	Sentinel lymph node	- Hot uptake in positive lymph nodes - Controversy on its utility
	ProSense	- Increases visualisation and detection of lymph nodes - Only animal trials
Bladder cancer	Raman spectroscopy	- Provides a noninvasive, real-time, and objective prediction of pathologic diagnosis - Only animal trials - Limited field of view
	PDD	- Increases detection of bladder tumours - Improves surgical resection - Reduces early recurrences - Better detection of CIS - Expensive - Not approved in several countries
	Virtual cystoscopy	- Low specificity - Images similar to those obtained via endoscopy - Higher diagnostic value - Available meta-analyses

5-ALA = 5-aminolevulinic acid; CIS = carcinoma in situ; FB = Fast Blue; FG = Fluoro-Gold; FR = Fluoro-Ruby; GFPRv = green fluorescent pseudorabies virus; GU = genitourinary; HIS = hyperspectral imaging; ICG = indocyanine green; NIRF = near-infrared fluorescence; NVB = neurovascular nerve bundle; PDD = photodynamic diagnosis; PSM = positive surgical margin; RVS = real-time virtual sonography; TRUS = transrectal ultrasound; US = ultrasound; WIT = warm ischaemia time.

Table 3 – Application of positron emission tomography to genitourinary tumours

GU tumour type	Molecular imaging	Purpose	Sensitivity, %	Specificity, %
Prostate cancer	18F-FDG PET	Staging	17–75	NA
	11C-choline PET	Staging	66–100	81–90
	11C-acetate PET	Staging	70–83	NA
Renal cancer	18F-FDG PET	Staging	47–90	80–100
Testicular cancer	18F-FDG PET	Staging	67–91	95–100
	18F-FDG PET	Treatment evaluation	80–100	67–100
	SPECT/CT	Treatment evaluation	NA	NA
Bladder cancer	18F-FDG PET	Staging	60–67	86–88
	11C-choline PET	Staging	NA	NA
	11C-methionine PET	Staging	78	NA

FDG = fluorodeoxyglucose; GU = genitourinary; MI = molecular imaging; NA = not applicable; PET = positron emission tomography; SPECT-CT = single-photon emission computed tomography in combination with computed tomography.

Fig. 2 – In vivo phase: manual navigation with separate screens [25].

technologies have the potential to fully integrate preoperative molecular images in the operating room. Previously acquired images, such as CT and MRI scans, can be formatted into 3D image sets and linked to sensors that track the position of surgical instrumentation, in real-time, relative to the image set [24–26].

By superimposing these images on a video-assisted view of the operative field (ie, during laparoscopic or robotic procedures), or by coregistering these images with other imaging modalities and fusing them into one augmented compound image, it is possible to improve the surgeon's ability to localise anatomic boundaries (Figs. 2 and 3). Providing AR information in the endoscopic view holds great promise for surgeons and represents a great challenge for AR researchers. This helps improve surgical accuracy.

For example, AR may enable rigid registration of an abdominal 3D patient model using radio-opaque markers stuck on the abdomen skin. The feasibility and benefits of this solution have been shown in both animals and humans [27,28]. However, at present, abdominal navigation systems are in experimental use and not yet perfected for daily surgical routine [29,30].

3.3. Application of image-guided genitourinary oncologic surgery

3.3.1. Adrenal tumours

The first use of AR technology for adrenal surgery was described by Marescaux et al. [31] during a case of laparoscopic right adrenalectomy with AR assistance for a benign adrenal tumour. Using 3D virtual reality proprietary software and 2-mm slice-enhanced spiral CT scanning, a 3D reconstruction of the lesion, the adrenal gland, and other intra-abdominal organs of the patient was provided in AR (Fig. 4). Advantages of the use of AR included delineation of dissection planes or resection margins and avoidance of injury to invisible structures, especially in the chosen moderately obese patient.

In 2011, Nicolau et al. [32] reported their initial experience with an interactive augmented reality (IAR) view during 15 malignant adrenal gland resections (Fig. 5). In all right

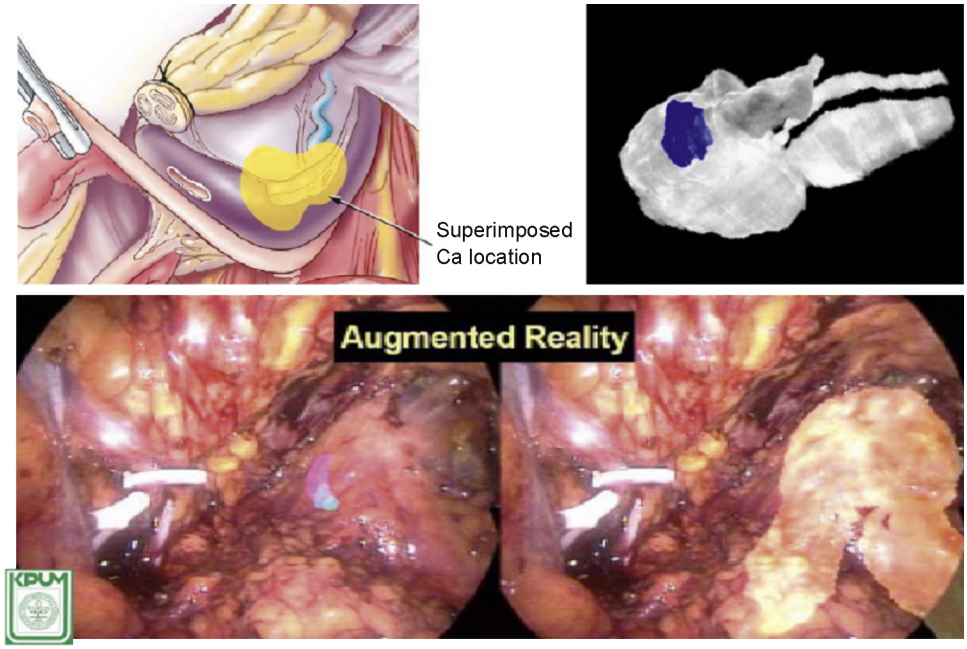

Fig. 3 – Nerve-sparing laparoscopic radical prostatectomy [22].

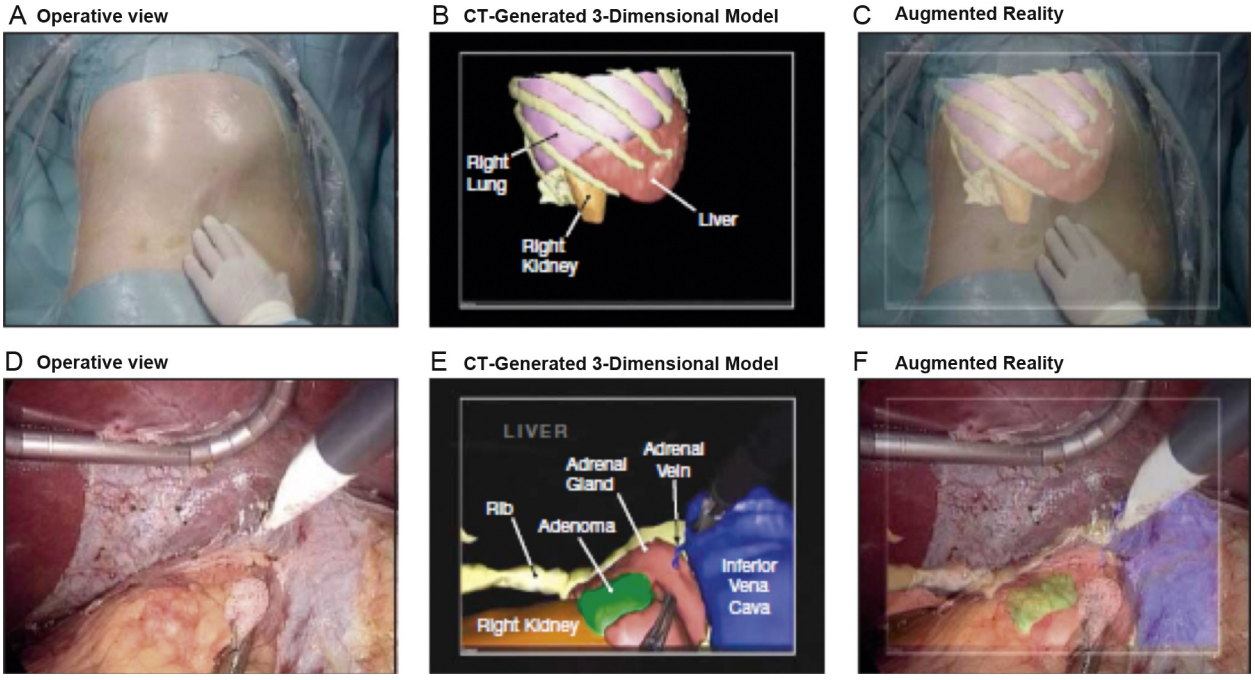

Fig. 4 – Augmented reality images of laparoscopic adrenalectomy [31]. CT = computed tomography.

adrenal glands, IAR provided a proper superimposition (maximal error of 2 mm). For left-sided procedures, this localisation was correct in two of the three cases. The transperitoneal left adrenal gland surgery is more complex, with the spleen being released from the abdominal wall and then rotated to allow the adrenal gland approach. The complexity of the procedure creates structure deformation, large variations in the organ position and shape, and complexity in finding or following internal landmarks like the spleen or arteria and vena lienalis. The authors noted there was a learning curve to learn 3D manipulation and anatomic landmark detection. After five IARs, time processing improved. Adrenal gland IAR results were efficient and accurate enough to guide the surgeon in the adrenal vein

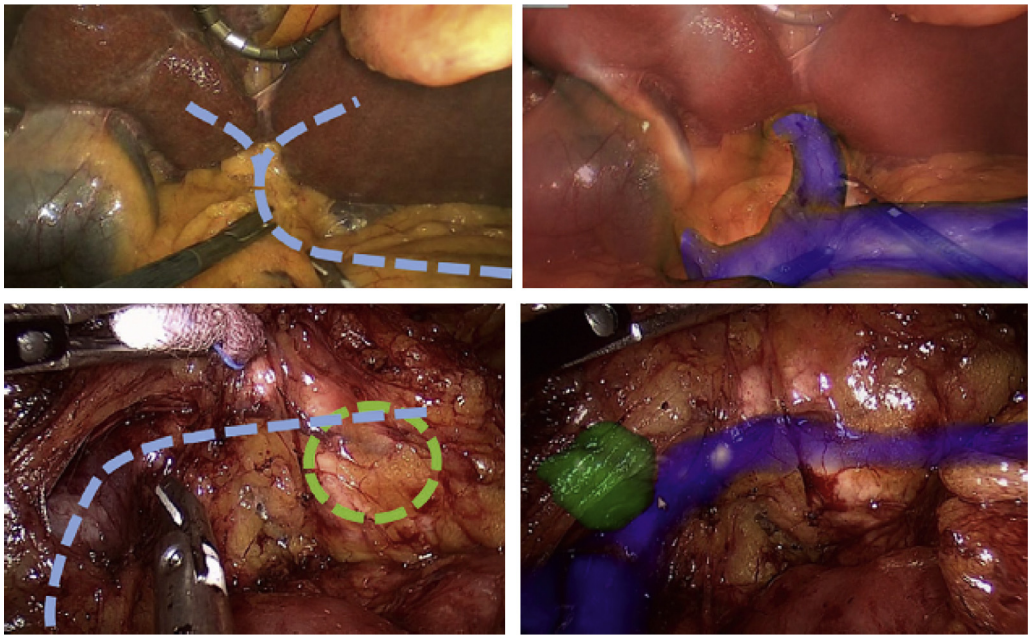

Fig. 5 – Correct estimation of vessels (blue) and tumour locations of the interactive augmented reality (IAR) (right views) during laparoscopic adrenalectomy. The first line shows a surgeon error of 45° in the orientation of right and left portal branch; the second line shows a surgeon erroneous location of the tumour (over 1 cm). In both cases IAR provides the correct location [32].

dissection and thus potentially reduce operative time and the risk of intraoperative complications.

3.3.2. Lymph node dissection for prostate cancer

One very practical clinical application where MI can help guide surgical intervention is the identification of lymph nodes (LNs) draining directly from the primary tumour (ie, sentinel lymph nodes [SLNs]) [33–43].

After intratumoural injection of a radiopharmaceutical agent, the carrier molecules cross the lymphatic pores and migrate into lymphatic vessels, and from there to the first echelon of LNs. The signals generated by the radiotracers are detected by extracorporeal scintigraphy and intraoperative scanning. For diagnosis, predictability of radiopharmaceutical transit time within the lymphatic vessels and up to the SLN is crucial [37]. Unfortunately, the pharmacokinetics and biodistribution of most NIR imaging agents, such as indocyanine green (ICG), cannot be monitored accurately [33].

To circumvent these problems, a hybrid radioactive and fluorescent radiocolloid (ICG-^{99m}Tc-NanoColl) [33–36,41] was recently developed to improve the surgical accuracy of laparoscopic LN dissection. A transrectal ultrasound (TRUS)-guided intraprostatic injection of the ICG-99mTc-NanoColl tracer was performed in patients with prostate carcinoma and with an increased risk of nodal metastasis [33]. The SLNs were preoperatively localised with lymphoscintigraphy and SPECT/CT and dissected, guided by a laparoscopic gamma probe and a fluorescence laparoscope (Fig. 6).

During the surgical procedure the SLNs could be identified in real-time using a combination of a gamma probe and a NIR-optimised fluorescence laparoscope [33]. In the prostatic fossa, the background ^{99m}Tc signal from the injection site prevents accurate gamma probe–based navigation to the preoperatively SPECT/CT-defined SLNs, but this shortcoming is compensated through the use of fluorescence. The hybrid nature of the tracer not only enables surgical guidance but also provides an opportunity to study the correlation between the location of tracer deposits within the prostate and the number and location of preoperatively visualised SLNs [34].

Generally, radioisotope-guided SLN dissection for prostate cancer has been reported to increase the sensitivity of detecting early metastases in open and laparoscopic pelvic LN dissection for prostate cancer, and thus it increases the prognosis and the overall survival of patients [34,37–39,43].

Jeschke et al. [37] presented their experience in laparoscopic radioisotope-guided SLN dissection performed in 140 patients with clinically localised prostate cancer preceding radical prostatectomy (RP). In 48.2% of the pelvic sidewalls (135 of 280), SLNs were exclusively outside the obturator fossa. Final histopathologic examination revealed SLN metastases in 19 patients (13.5%); 71.4% of the detected metastases (20 of 28) were outside the current standard of lymph node dissection (LND) limited to the obturator fossa.

The concept of SND in prostate cancer is compelling because it saves operative time and provides lower morbidity due to extensive LND. However, intratumoural injection of a tracer is necessary, but identification of index lesions, especially using TRUS, is unreliable. Thus tracer distribution in the LNs reflects more prostate drainage than tumour drainage.

3.3.3. Prostate cancer

3.3.3.1. Intraoperative navigation. Surgical therapy for clinically localised prostate cancer has undergone a significant transition in the past several decades. With wide application of minimally invasive RP, there has been a renewed interest in image-guided navigation techniques that could

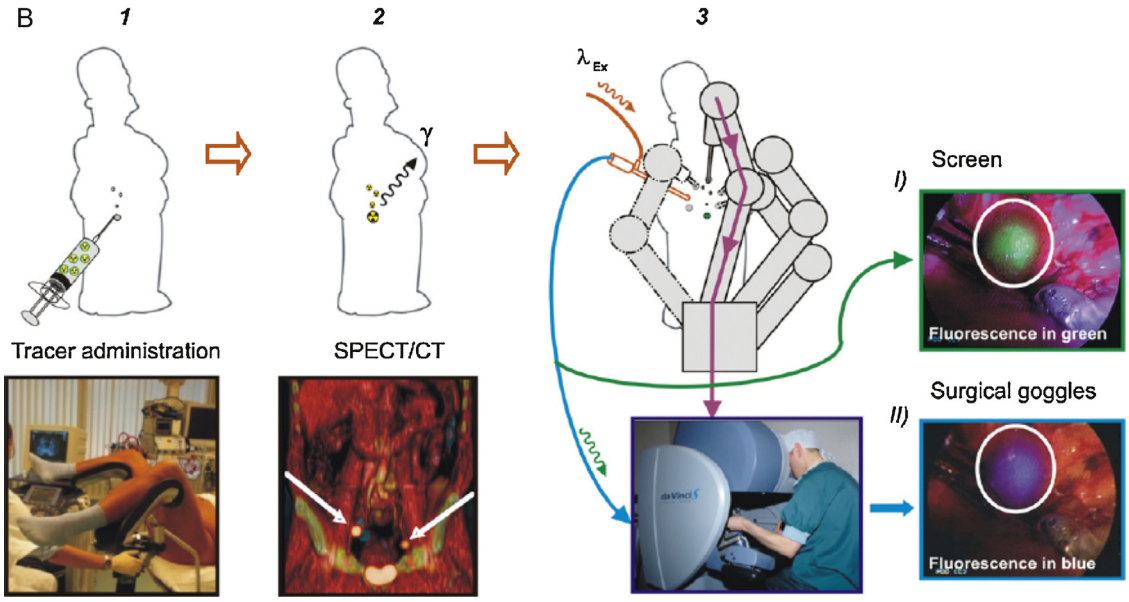

Fig. 6 – Intraoperative laparoscopic fluorescence guidance to the sentinel lymph node in prostate cancer patients [33]. SPECT/CT = single-photon emission computed tomography combined with computed tomography.

potentially be used to supplement the tumour resection and visualisation/preservation of neurovascular bundles (NVBs). Although this area of research is still in its infancy, these imaging techniques hold significant promise in achieving the ultimate goals of RP [44–49].

Several studies have investigated the role of TRUS to guide the surgeon during RP, and duplex US has been used to identify the blood flows within the NVBs [22,44–47].

Ukimura et al. [46] used real-time power Doppler TRUS to image the NVBs intraoperatively and reported that real-time TRUS helps identify the anatomic course of the NVBs, measures the number of visible vessels, and quantifies the arterial blood flow resistive index in the NVBs.

In 2008, van der Poel et al. [47] found TRUS with duplex to be helpful in visualising the NVBs during release of the prostatic apex, identifying hypoechoic prostatic nodules, guiding areas of suspected extracapsular extension, and facilitating division of the posterior bladder neck. The authors also reported a lower rate of positive surgical margins (PSMs) with the use of TRUS during LRP and suggested that visualisation with this technology allowed for a more complete dissection and better cancer control as well as improved potency recovery [47]. This approach, although innovative, posed several challenges. For example, operator dependency, variability in probe positioning, and low resolution for defining microscopic structures are the main drawbacks of this technique, resulting in its very limited use [46].

An AR navigation system that conveys virtual organ models generated from TRUS onto a real laparoscopic video during RP has been described [45–49]. This system uses custom-developed needles with coloured pins inserted into the prostate as soon as the organ surface is uncovered. By tracing the navigation aids in real-time, it allowed a registration between the TRUS image and laparoscopic video based on the 2D and 3D point correspondences. With this registration, the system correctly superimposed TRUS-based 3D information on an additional AR monitor placed next to the normal laparoscopic screen.

This first in vivo human application of the surgical navigation system in LRP was successful. No complications occurred, the prostate was removed together with the navigation aids, and the system supported the surgeons as intended with AR visualisation in real-time [48].

In 2007, Davila et al. evaluated whether fluorescent tracers could consistently label the NVBs and major pelvic ganglion after intracavernosal penile injection and thus facilitate nerve sparing during RP [50]. Male Sprague-Dawley rats received penile injections of deionised water, Fluoro-Gold (FG), Fast Blue, Fluoro-Ruby, or green fluorescent pseudorabies virus (Fig. 7). The authors demonstrated that injecting FG into the rat penis 2–3 d before pelvic surgery might help identify the NVBs under fluorescent light, proposing FG as a nerve tracer during pelvic surgery in animals. Although this technology never took off, it can still be considered highly valuable during surgery.

Technologies to improve the accuracy of prostate biopsy are rapidly emerging. Recently, a 3D prostate biopsy tracking and targeting device was described, allowing biopsy-site tracking for future recall and fusion of MRI targets with real-time US, thus improving current methods for diagnosis and follow-up of prostate cancer [51]. Although promising, these early experiences have not yet conclusively shown the benefit of tracking and targeted biopsy with MR fusion.

3.3.3.2. Oncologic resection. Because a PSM is associated with a higher rate of biochemical recurrence, it is a challenging concept to make the tumour visible during surgery to reduce the risk of a PSM. Targeted fluorescent compounds may help illuminate cancerous tissue.

In 2009, Adam et al. [52] reported the first prospective study to investigate the feasibility of intraoperative identification of PSMs during open retropubic or endoscopic extraperitoneal RP. Thirty-nine patients received 20 mg/kg of body weight of 5-ALA orally and underwent laparoscopic and open RP. A PDD-suitable laparoscopy optic was used.

There were more false-negative cases in the open group (four vs two) than in the endoscopic group but more false-positive cases in the endoscopic group (two vs none) than in the open group. PDD with 5-ALA–induced protoporphyrin IX proved to be a feasible and effective method for reducing

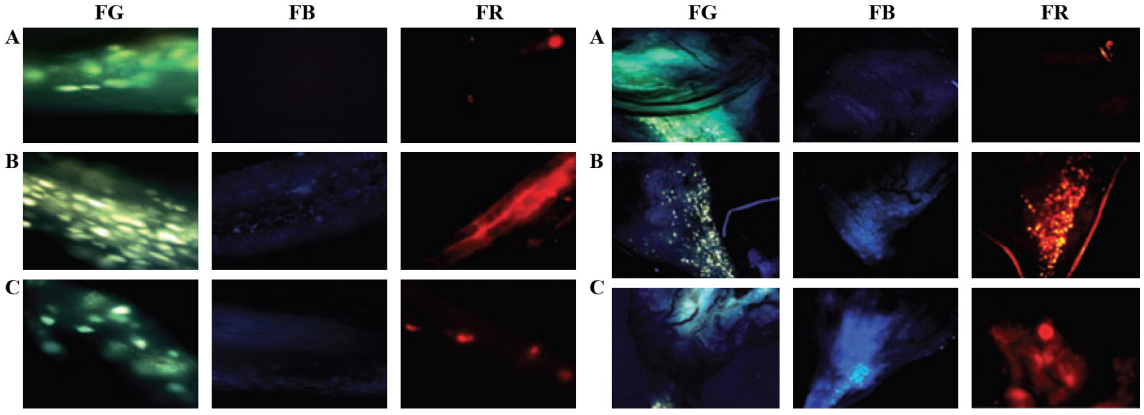

Fig. 7 – Visualisation of the neurovascular bundles and major pelvic ganglion (A) 2 d, (B) 3 d, and (C) 14 d after penile injection with Fluoro-Gold (FG), Fast Blue (FB), and Fluoro-Ruby (FR) [50].

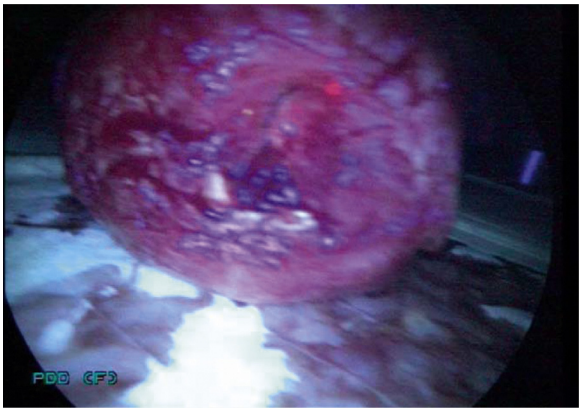

Fig. 8 – Prostate under photodynamic diagnosis [52].

the rate of PSMs, with a higher sensitivity during LRP (Fig. 8).

Several imaging modalities can potentially enhance the minimally invasive prostatectomy with promising outcomes in cancer control and NVB sparing. Although the clinical experience is still limited, studies with higher patient volumes and further development of the technique seem justified.

Brouwer et al. recently described one clinical pilot case to illustrate how intraoperative navigation based on preoperative 3D scintigraphic images may help improve the efficacy of endoscopic hybrid radio- and fluorescence-guided surgery for prostate cancer [26]. This study could demonstrate the feasibility of combined rigid navigation based on preoperative SPECT/CT images and intraoperative fluorescence imaging for soft tissue navigation within a small range of deformation in complex surgical procedures like robot-assisted laparoscopic RP.

When combined with the use of hybrid (radioactive and fluorescent) tracers, such a navigation setup enabled preoperative surgical planning as well as intraoperative navigation toward the lesions using the radioactive signature, while accurate target localisation and visualisation could take place using the fluorescent signature [26].

3.3.3.3. Application of positron emission tomography imaging for surgery. Several studies described the application of PET for prostate cancer. In 2005, in a direct comparison between ^{11}C-choline PET and MR imaging and MR spectroscopy for the diagnosis and staging of prostate cancer, 11C-choline PET had a sensitivity of 100% for primary lesions, whereas the sensitivities of MR imaging and MR spectroscopy were 60% and 65%, respectively. Regarding the localisation of primary lesions, 11C-choline PET results agreed with pathologic findings in 13 patients (81%) [53].

Another study used PET/CT with ^{11}C-choline in 43 patients with known prostate cancer prior to RP [54]. ^{11}C-choline PET/CT revealed a sensitivity of 83% for localisation of nodules >5 mm, which was comparable with TRUS-guided biopsy. The authors found no relevant information regarding the detection of extraprostatic tumour extension, which might be explained by the limited resolution of PET imaging.

Initial preclinical and clinical studies showed that ^{18}F-fluorocholine is a promising tracer for the evaluation of primary and metastatic prostate cancer [4,55]. In a study including 100 patients with a persistent increase in serum prostate-specific antigen levels after RP, radiotherapy, or hormonal therapy, ^{18}F-fluorocholine PET/CT results had a significant impact on detecting local recurrences and LN metastases [4,55].

3.3.4. Kidney cancer

The widespread use of modern imaging methods has led to the earlier diagnosis and improved staging of renal cell carcinoma (RCC), resulting in a marked increase in the number of renal tumours detected incidentally. In this context, nephron-sparing surgery (NSS) offers a good therapy for small renal lesions, but it requires adequate intraoperative tumour demarcation [56].

3.3.4.1. Intraoperative navigation and renal tumour imaging. Intraoperative imaging techniques that enhance viewing of the operative field might provide better discrimination between tumour tissue and normal renal parenchyma and thus reduce the risk for PSMs [57–59].

NIRF angiography after ICG administration allows for a detailed look at the anatomy of the vascular system and has been used to distinguish renal tumours from normal tissue by highlighting the renal vasculature (Fig. 9). This technology has shown the potential to maximise oncologic control and nephron sparing during open and robotic partial nephrectomy [58,59].

In 2009, Teber et al. described a novel soft-tissue navigation system developed to enhance the surgeon's perception and to provide decision-making guidance directly before initiation of kidney resection for laparoscopic partial nephrectomy (LPN) [25]. During the soft tissue navigation, the navigation aids, a mobile C-arm capable of cone-beam imaging, and a standard personal computer were used. The navigation procedure was divided into these basic steps: preoperative planning, insertion of navigation aids, planning registration, and real-time inside-out tracking and visualisation. New 3D virtual images of the kidney with neighbouring anatomic structures were created and visualised as an AR overlay of the endoscopic video image. An independent operator manually combined the reconstructed transparent 3D CT images with the real-time video-endoscopic images. Under AR guidance, the renal vessels and renal tumours were found through the surrounding fat under AR guidance (Fig. 10), and tumour-free margins were obtained in all patients.

In a related study, Su et al. investigated a marker-less tracking system for real-time stereo-endoscopic visualisation of preoperative CT imaging as an augmented display during robot-assisted LPN [60]. After generating a 3D surface model of the kidney, tumour, and collecting system from the preoperative CT images, the 3D segmented kidney model was then imported into the endoscopic video segment as an overlay. The tracking-system used an

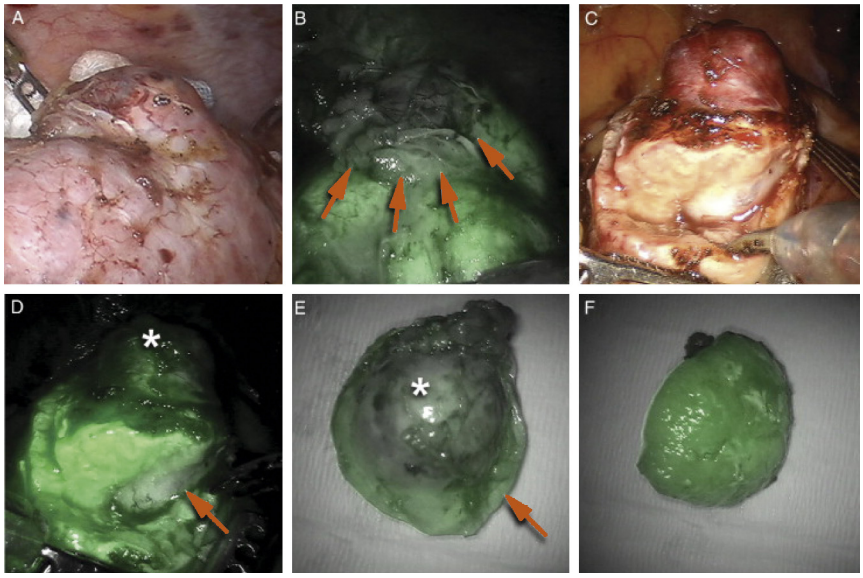

Fig. 9 – Renal lesion identification. In contrast to (A) standard white-light imaging, (B) margin (arrows) between fluorescent normal parenchyma and clear cell renal cell carcinoma was readily apparent. (C) Resection of clear cell renal cell carcinoma was seen with white light. (D) Same lesion viewed with near-infrared fluorescence (NIRF), with cap of fluorescent normal parenchyma (asterisk) seen overlying hypofluorescent tumour (arrow). (E,F)This helped obtain negative margin during resection of endophytic portion of tumour, which was also seen with NIRF after resection [58].

automatic registration algorithm, for which several points on the kidney surface surrounding the renal mass were selected as fixed reference points. Triangulation methods were used to calculate the 3D positions of the points on the surface of the kidney and compute the corresponding orientation and position changes of the 3D model overlay. Finally, the system refined the registration using a modified 3D-to-3D iterative closest point registration. In this way, the authors could track the kidney surface in real-time by applying intraoperative video recordings and semitransparent AR overlays of 3D models of the kidney, the tumour, and the collecting system (Fig. 11).

3.3.4.2. Use of fluorescence. The application of fluorescence to improve tumour control and decrease PSMs has been also investigated for renal surgery [59,60]. In 2009, Hoda et al. [61] reported their experience with PDD after oral administration of 5-ALA for assessment of tumour type and surgical margins in LPN (Fig. 12). PDD with 5-ALA was able to predict the type of the lesion with an accuracy of 94% and with a positive predictive value of 98%. PDD with 5-ALA also identified both cases with positive resection margins, which were confirmed on histologic examinations.

A hyperspectral imaging (HSI) technique was recently applied to monitor renal oxyhemoglobin noninvasively during partial nephrectomy, thus facilitating intraoperative decision making and protecting kidney function (Fig. 13) [62–64].

In this way, the application of the HSI technique could evaluate the renal oxygenation profiles, demonstrating that artery-only clamping improves renal oxygenation relative to complete hilar occlusion during NSS. This could be associated with a shorter warm ischaemia time during the tumour resection [63].

3.3.4.3. Use of image-fusion techniques. Percutaneous image-guided tumour ablation has an increasingly prominent role as a minimally invasive treatment for renal tumours. Precise cryoprobe placement is essential for successful ablation [65].

Real-time virtual sonography (RVS) displays split-screen images of the CT/MRI images with the intraoperative real-time US image. Applying this technology in percutaneous radiofrequency ablation and/or percutaneous cryosurgery for RCC, for example, RVS compensated for conventional US limitations by reducing the difficulty of interpretation of the lower resolution US image, achieving a better understanding of the prenephrectic anatomy, and helping understand the hidden anatomy beneath the US interface such as gas or bone [65].

The detection of RCC with PET imaging is hampered by the fact that most radiotracers are excreted via the kidneys. Nevertheless, the renal elimination of fluorodeoxyglucose (^{18}F-FDG) can in part be overcome by increasing diuresis with hydration or by administering diuretics [4].

The largest series so far included 66 patients who underwent 90 ^{18}F-FDG-PET scans for suspected or known RCC [66]. ^{18}F-FDG-PET demonstrated a sensitivity of 60% compared with 91.7% for CT and was less sensitive in detecting primary tumours, retroperitoneal LN metastases, or distant metastases. The specificity was 100% for both modalities.

3.3.5. *Testicular cancer*

Retroperitoneal lymph node dissection (RPLND) represents an integral part of the treatment of men with high-risk or metastatic testicular cancer. Nevertheless, only a few studies investigating the application of image-guided surgery in RPLND are available [67,68].

In 2002, Ohyama et al. presented the first study on the detection of SLNs with radioactive tracer in patients with

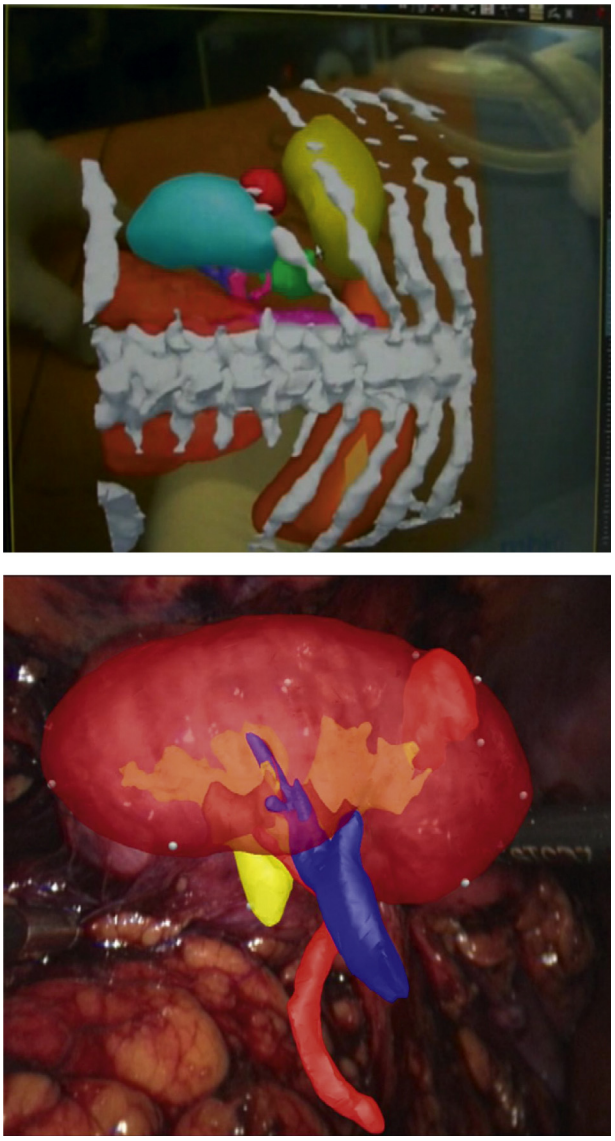

Fig. 10 – Using augmented reality for ideal port placement and identification of renal tumours during laparoscopic partial nephrectomy [25].

clinical stage I testicular tumour [67]. SLNs could be detected in all patients examined on static imaging. In right tumours, hot uptakes were observed at the inter-aortocaval, paracaval, or common iliac region; for left tumours, positive uptakes were detected in the para-aortic region (Fig. 14).

Nevertheless, the utility of SLN identification in testicular tumours is controversial with limited research on this topic. Penna et al. investigated the utility of fluorescent MI with the enzymatically cleaved probe ProSense [68].

ProSense is an activatable fluorescent MI agent that demonstrates changes in the levels of protease (cathepsin) activity, which are present and detectable in normal states but further concentrated in diseased states including oncologic diseases. Cleavage by cathepsin led to a fluorescent signature enabling more definitive LN visualisation during RPLND in animal models [68]. After all visualised LNs were excised, the NIR fluorescence detector was used to identify any residual LNs (Fig. 15). This concept may have significant potential in testicular cancer and other GU organ types.

3.3.5.1. Testicular cancer and positron emission tomography imaging. In patients with stage I seminoma, the results of FDG-PET for LN staging were similar to CT, whereas FDG-PET detected metastases in stage I nonseminomatous germ cell tumour in the presence of negative staging CT and tumour markers [4,69]. The sensitivity, specificity, and accuracy of PET were 70%, 100%, and 93%, respectively. The sensitivity of detecting small retroperitoneal metastases was 88%. The negative and positive predictive values were 92% and 100%, respectively, whereas the negative predictive value of standard staging procedures was only 78%.

The use of SPECT/CT enables accurate anatomic localisation of retroperitoneal SLNs in patients with testicular cancer, facilitating their laparoscopic retrieval. Real-time image guidance by a portable gamma camera improves intraoperative SLN detection and appears to identify (20%) additional SLNs [70].

Further studies on humans testing the applicability of MI techniques for testicular cancer are ongoing.

3.3.6. *Bladder cancer*

Determining the depth of bladder tumour invasion into the bladder wall is an important factor in tumour staging and treatment. Currently, this is assessed by cystoscopic transurethral tumour resection, which is invasive and may be associated with tumour understaging in many cases [6]. New developments in optical diagnostics have a potential for less invasive and improved detection of bladder cancer [71]. Raman spectroscopy (RS) enables the measurement of molecular components of tissue in a qualitative and quantitative way. The principle of this optical technique is based on the Raman effect, or inelastic scattering, resulting in a different wavelength of the scattered light.

All of the shifted wavelengths from the various molecules in tissue combine to form the Raman spectrum, which is a function of the molecular composition of the tissue investigated. This molecular composition changes if pathologic transformations occur, and thus RS can provide an objective prediction of pathologic diagnosis. To assist with interpretation of RS, a pseudo-colour map of the tissue under examination can be created. Tissue areas with similar spectra, and therefore with similar molecular composition, are depicted in the same colour, thus creating a picture comparable with histopathology. Several groups have determined the diagnostic accuracy of RS for bladder cancer, reporting sensitivity and specificity of 90–95% and 94–98%, respectively [71,72]. The potential advantage of RS is its ability to provide a noninvasive, real-time, and objective prediction of pathologic diagnosis. Nevertheless, because RS has a limited field of view, screening the entire bladder is too time consuming; therefore, RS must be targeted at visually suspicious lesions [71,72].

The application of fluorescence to improve tumour control has achieved great success for investigating bladder

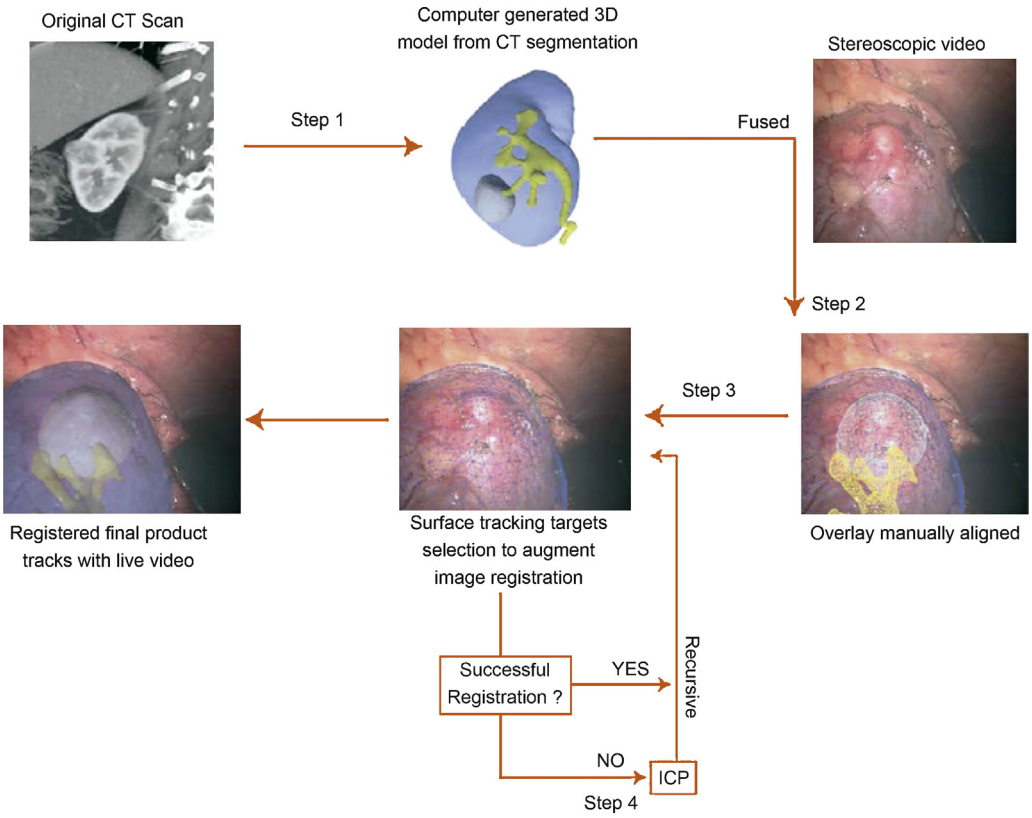

Fig. 11 – Flowchart displaying steps needed to achieve successful three-dimensional registration of preoperative computed tomography (CT) image to live stereoscopic video [60]. ICD = iterative closest point.

cancer [71,73]. PDD, also referred to as fluorescence cystoscopy, is an optical technique using fluorescence as a contrast mechanism to indicate pathologic tissue (Fig. 16). PDD offers the additional detection of patients with non–muscle-invasive bladder cancer and less residual tumour and longer recurrence-free survival [73].

In previous reports, the sensitivity of PDD and WLC ranged from 82% to 97% and from 62% to 84%, respectively [74]. The benefit of PDD was highest in carcinoma in situ (CIS). It has become evident that PDD detects more tumour lesions and less residual tumour occurs after PDD-guided transurethral resection (TUR) compared with WLC [73–75]. Although a clear benefit for PDD has been found for the detection of CIS, the value of this technique with respect to CIS recurrences and progression remains unclear.

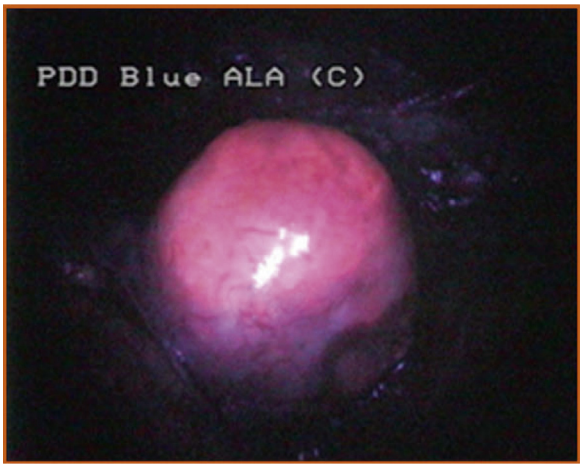

Fig. 12 – Red fluorescence of the resected tumour under blue light [61].

A recent study evaluated the impact of hexaminolevulinate fluorescence cystoscopic detection of papillary non–muscle-invasive bladder cancer on the long-term recurrence rate [76]. In a cohort of 516 patients, the median time to recurrence was 9.4 mo in the white-light group and 16.4 mo in the fluorescence group. Hexaminolevulinate fluorescence cystoscopy reported improved long-term bladder cancer time to recurrence with a trend towards improved bladder preservation.

Future studies will have to show if the intervals to follow-up cystoscopies can be altered when PDD is used and if PDD changes adjuvant treatment, for instance, due to the safe exclusion of CIS. The necessity of re-TUR after PDD must also be evaluated [73]. The combination of PDD with optical coherence tomography may be promising.

Narrow-band imaging (NBI) is an optical image enhancement technique designed for endoscopy to enhance the contrast between mucosal surfaces and microvascular structures without the use of dyes (Fig. 17) [71]. Up to date, only a few studies assessing the value of NBI in bladder cancer have been published [71,77–79]. Herr et al. performed WLC with subsequent NBI cystoscopy in 427 consecutive patients with a history of non–muscle-invasive

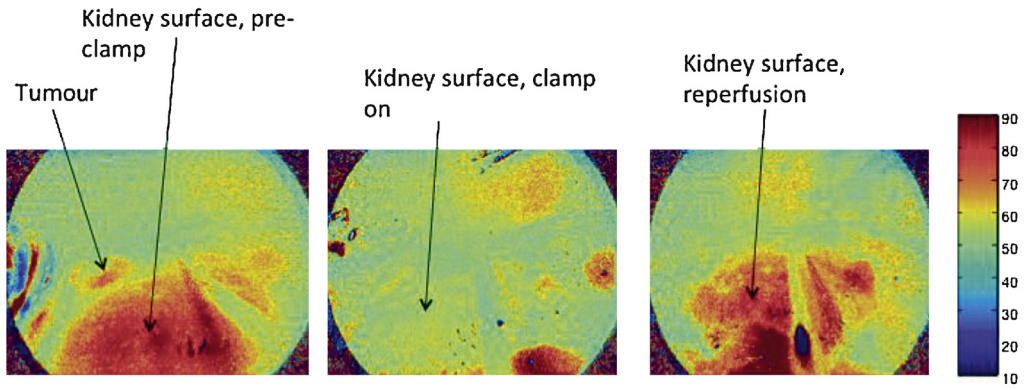

Fig. 13 – Colour-coded kidney surface oxygenation maps [64].

bladder cancer. Recurrence was found in 103 patients. In 56% of patients with a recurrence, additional tumours were detected by NBI, and in 12% of patients the bladder tumours were detected only due to NBI. For WLC and NBI cystoscopy, the overall sensitivity was 87% and 100% and the overall specificity was 85% and 82%, respectively [77].

The elimination of ^{18}F-FDG via the efferent urinary tracts represents a significant limitation of ^{18}F-FDG-PET for the evaluation of a primary bladder tumour [4]. Nevertheless, the addition of metabolic information from FDG to the anatomic information from CT yielded improved diagnostic accuracy in the preoperative staging of invasive bladder carcinoma, with a sensitivity, specificity, and accuracy of 60%, 88%, and 78%, respectively [4,80].

Over the past decade, technical developments in CT and MR imaging have made it possible to produce an

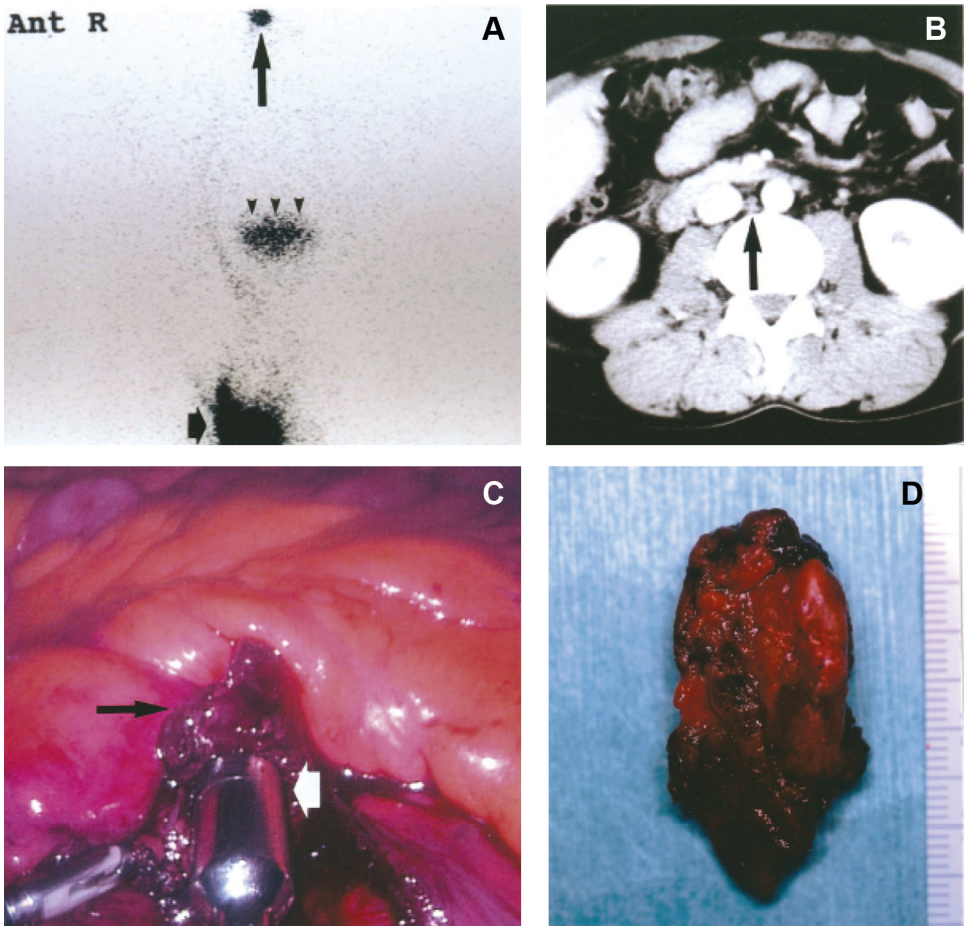

Fig. 14 – (A) Sentinel lymph node (arrow) on static image; (B) sentinel lymph node is indicated by arrow; (C) intraoperative search for sentinel lymph node (arrow) with laparoscopic handheld gamma detection probe (white arrow); (D) removed specimen [67].

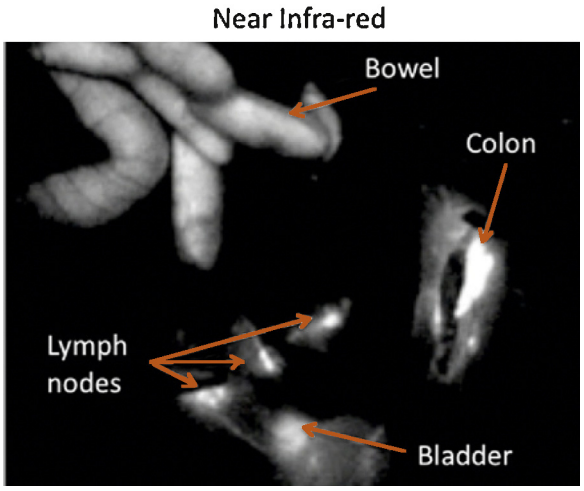

Fig. 15 – Exposure for retroperitoneal lymph node dissection in guinea pig under ProSense [68].

endoluminal view of hollow organs. These techniques have yielded images that are similar to those obtained via endoscopy. These imaging protocols allow patients to undergo a "virtual endoscopy" or, in the case of bladder cancer, virtual cystoscopy (via either CT virtual cystoscopy [CTVC] or MR virtual cystoscopy [MRVC]) [81,82]. A recent meta-analysis investigating studies evaluating the diagnosis validity of virtual cystoscopy and US showed that both CTVC and MRVC were better imaging methods for diagnosing bladder cancer than US. CTVC has a higher diagnostic value (sensitivity, specificity, and diagnostic odds ratio) for the detection of bladder cancer than either MRCT or US [82].

3.3.7. *Future prospects*

Innovative TRUS-based techniques were recently proposed for the noninvasive detection of prostate cancer. HistoScanning (HS) technology uses information from backscattered ultrasonographic raw data (ie, the native radiofrequency data) that are processed by a set of tissue-characterisation algorithms. HS has two main advantages. It visualises cancerous lesions, and thus provides anatomic pictures useful for surgery planning, and it allows side-specific prediction. An improvement in HS technology is likely to increase the capacity to characterise prostate tissues in the vicinity of NVBs [83].

Diffusion-tensor imaging (DTI) is an MR-based imaging technique that can be used to map the orientation of axon fibres using a technique termed *DTI tractography* [84]. A recent study evaluated the feasibility of DTI tractography of the prostate for mapping of the periprostatic neurovascular anatomy.

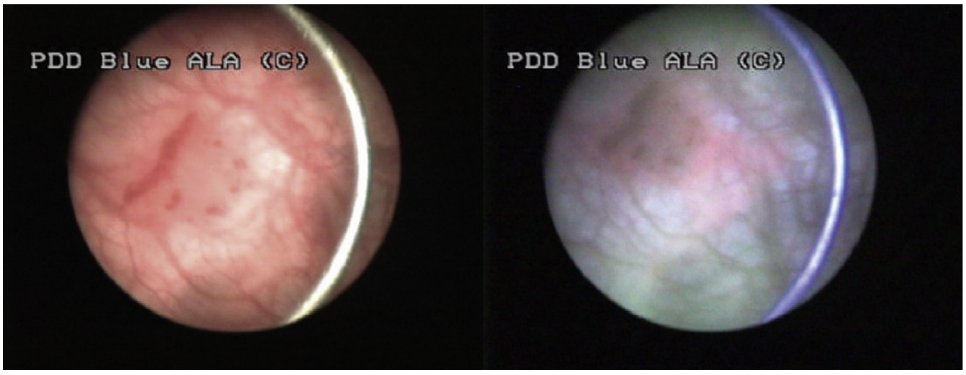

Fig. 16 – Photodynamic diagnosis (PDD): detection of carcinoma in situ with white light on the left and PDD on the right [71].

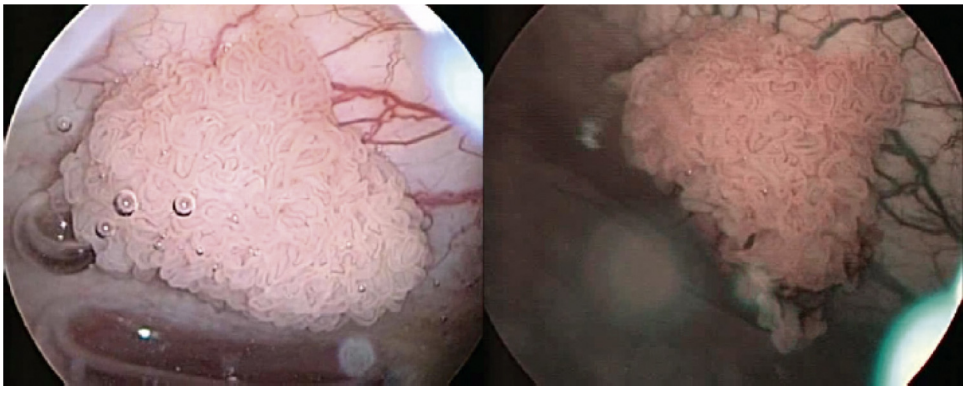

Fig. 17 – Narrow-band imaging (NBI): detection of a papillary bladder tumour with white light on the left and NBI on the right [71].

DTI tractography of the prostate elucidated an exquisite level of periprostatic fibre tract detail, and fibre tracts were visualised along the entire border of the prostate with similar tract density [84].

Although the preliminary data are encouraging, randomised studies to validate these initial promising findings are needed for those technologies that may be available at a larger scale in the near future.

4. Conclusions

Image-guided surgery is likely to be of increasing importance in the near future as treatments for urologic malignancies become more molecularly targeted. Within the field of urology, fluorescence guidance, surgical navigation, and AR techniques hold promise for intraoperative identification of SLNs, anatomic structures, and tumour lesions.

Although an increased number of studies report on the application of PDD, PET, and NIRF with ICG for urologic malignancies, the research and development of surgical navigation is still in an experimental phase.

Laparoscopic and robotic challenges lie in the further optimisation of targeted and/or activatable (hybrid) imaging agents and the integration between imaging agents and camera systems, thereby enabling more accurate fluorescence image guidance during surgical interventions, thus improving the detection and the therapy of all urologic tumours and enhancing intraoperative GU oncologic surgery.

Author contributions: Francesco Greco had full access to all the data in the study and takes responsibility for the integrity of the data and the accuracy of the data analysis.

Study concept and design: Greco, Rassweiler.
Acquisition of data: Greco.
Analysis and interpretation of data: Greco.
Drafting of the manuscript: Greco.
Critical revision of the manuscript for important intellectual content: Cadeddu, Gill, Kaouk, Remzi, Thompson, van Leeuwen, van der Poel, Fornara, Rassweiler.
Statistical analysis: None.
Obtaining funding: None.
Administrative, technical, or material support: None.
Supervision: Rassweiler.
Other (specify): None.

Financial disclosures: Francesco Greco certifies that all conflicts of interest, including specific financial interests and relationships and affiliations relevant to the subject matter or materials discussed in the manuscript (eg, employment/affiliation, grants or funding, consultancies, honoraria, stock ownership or options, expert testimony, royalties, or patents filed, received, or pending), are the following: None.

Funding/Support and role of the sponsor: None.

References

[1] Ntziachristos V. Going deeper than microscopy: the optical imaging frontier in biology. Nat Methods 2010;7:603–14.
[2] Bouchelouche K, Oehr P. Recent developments in urologic oncology: positron emission tomography molecular imaging. Curr Opin Oncol 2008;20:321–6.
[3] Bouchelouche K, Oehr P. Positron emission tomography and positron emission tomography/computerized tomography of urological malignancies: an update review. J Urol 2008;179:34–45.
[4] Powles T, Murray I, Brock C, Oliver T, Avril N. Molecular positron emission tomography and PET/CT imaging in urological malignancies. Eur Urol 2007;51:1511–21, discussion 1520–1.
[5] Rioja J, Rodríguez-Fraile M, Lima-Favaretto R, et al. Role of positron emission tomography in urological oncology. BJU Int 2010;106:1578–93.
[6] Gee MS, Harisinghani MG, Tabatabaei S. Molecular imaging in urologic surgery. Urol Clin North Am 2009;36:125–32.
[7] Piston DW, Masters BR, Webb WW. Three-dimensionally resolved NAD(P)H cellular metabolic redox imaging of the in situ cornea with two-photon excitation laser scanning microscopy. J Microsc 1995;178:20–7.
[8] Pham TH, Bevilacqua F, Spott T, Dam JS, Tromberg BJ, Andersson-Engels S. Quantifying the absorption and reduced scattering coefficients of tissue-like turbid media over a broad spectral range with noncontact Fourier transform hyperspectral imaging. Appl Opt 2000;39:6487–97.
[9] van den Berg NS, van Leeuwen FW, van der Poel HG. Fluorescence guidance in urologic surgery. Curr Opin Urol 2012;22:109–20.
[10] Larson SM, Schöder H. Advances in positron emission tomography applications for urologic cancers. Curr Opin Urol 2008;18:65–70.
[11] Liberati A, Altman DG, Tetzlaff J, et al. The PRISMA statement for reporting systematic reviews and meta-analyses of studies that evaluate health care interventions: explanation and elaboration. Ann Intern Med 2009;151:W65–94.
[12] Barkun JS, Aronson JK, Feldman LS, et al. Evaluation and stages of surgical innovations. Lancet 2009;374:1089–96.
[13] Thakur ML, Lentle BC. SNM; Radiological Society of North America (RSNA). Joint SNM/RSNA Molecular Imaging Summit Statement. J Nucl Med 2005;46:11N–3N, 42N.
[14] Mankoff DA. A definition of molecular imaging. J Nucl Med 2007;48:18N.
[15] Coleman J, Nascimento R, Solomon SB. Advances in imaging for urologic procedures. Nat Clin Pract Urol 2007;4:498–504.
[16] Weissleder R, Ntziachristos V. Shedding light onto live molecular targets. Nat Med 2003;9:123–8.
[17] Bogaards A, Sterenborg HJ, Trachtenberg J, Wilson BC, Lilge L. In vivo quantification of fluorescent molecular markers in real-time by ratio imaging for diagnostic screening and image-guided surgery. Lasers Surg Med 2007;39:605–13.
[18] Keereweer S, Kerrebijn JD, van Driel PB, et al. Optical image-guided surgery—where do we stand? Mol Imaging Biol 2011;13:199–207.
[19] Baumhauer M, Feuerstein M, Meinzer HP, et al. Navigation in endoscopic soft tissue surgery: perspectives and limitations. J Endourol 2008;22:751–66.
[20] Crow P, Stone N, Kendall CA, Persad RA, Wright MP. Optical diagnostics in urology: current applications and future prospects. BJU Int 2003;92:400–7.
[21] Zaak D, Karl A, Knuchel R, et al. Diagnosis of urothelial carcinoma of the bladder using fluorescence endoscopy. BJU Int 2005;96:217–22.
[22] Ukimura O. Image-guided surgery in minimally invasive urology. Curr Opin Urol 2010;20:136–40.
[23] Li G, Cuilleron M, Cottier M, et al. The use of MN/CA9 gene expression in identifying malignant solid renal tumors. Eur Urol 2006;49:401–5.
[24] Nascimento RG, Coleman J, Solomon SB. Current and future imaging for urologic interventions. Curr Opin Urol 2008;18:116–21.
[25] Teber D, Guven S, Simpfendörfer T, et al. Augmented reality: a new tool to improve surgical accuracy during laparoscopic partial nephrectomy? Preliminary in vitro and in vivo results. Eur Urol 2009;56:332–8.

[26] Brouwer OR, Buckle T, Bunschoten A, et al. Image navigation as a means to expand the boundaries of fluorescence-guided surgery. Phys Med Biol 2012;57:3123–36.
[27] Mårvik R, Langø T, Tangen GA, et al. Laparoscopic navigation pointer for 3D image guided surgery. Surg Endosc 2004;18:1242–8.
[28] Feuerstein M, Mussack T, Heining SM, Navab N. Intraoperative laparoscope augmentation for port placement and resection planning in minimally invasive liver resection. IEEE Trans Med Imaging 2008;27:355–69.
[29] Teber D, Baumhauer M, Guven EO, Rassweiler J. Robotic and imaging in urological surgery. Curr Opin Urol 2009;19:108–13.
[30] Rassweiler J, Baumhauer M, Weickert U, et al. The role of imaging and navigation for natural orifice transluminal endoscopic surgery. J Endourol 2009;23:793–802.
[31] Marescaux J, Rubino F, Arenas M, Mutter D, Soler L. Augmented reality–assisted laparoscopic adrenalectomy. JAMA 2004;292:2214–5.
[32] Nicolau S, Soler L, Mutter D, Marescaux J. Augmented reality in laparoscopic surgical oncology. Surg Oncol 2011;20:189–201.
[33] van der Poel HG, Buckle T, Brouwer OR, Valdés Olmos RA, van Leeuwen FWB. Intraoperative laparoscopic fluorescence guidance to the sentinel lymph node in prostate cancer patients: clinical proof of concept of an integrated functional imaging approach using a multimodal tracer. Eur Urol 2011;60:826–33.
[34] Buckle T, Brouwer OR, Valdés Olmos RA, van der Poel HG, van Leeuwen FW. Relationship between intraprostatic tracer deposits and sentinel lymph node mapping in prostate cancer patients. J Nucl Med 2012;53:1026–33.
[35] Buckle T, Chin PT, van Leeuwen FW. (Non-targeted) radioactive/fluorescent nanoparticles and their potential in combined pre- and intraoperative imaging during sentinel lymph node resection. Nanotechnology 2010;21:482001.
[36] van Leeuwen AC, Buckle T, Bendle G, et al. Tracer-cocktail injections for combined pre- and intraoperative multimodal imaging of lymph nodes in a spontaneous mouse prostate tumor model. J Biomed Opt 2011;16:016004.
[37] Jeschke S, Beri A, Grüll M, et al. Laparoscopic radioisotope-guided sentinel lymph node dissection in staging of prostate cancer. Eur Urol 2008;53:126–33.
[38] Jeschke S, Lusuardi L, Myatt A, Hruby S, Pirich C, Janetschek G. Visualisation of the lymph node pathway in real time by laparoscopic radioisotope- and fluorescence-guided sentinel lymph node dissection in prostate cancer staging. Urology 2012;80:1080–6.
[39] Häcker A, Jeschke S, Leeb K, et al. Detection of pelvic lymph node metastases in patients with clinically localized prostate cancer: comparison of [18F]fluorocholine positron emission tomography-computerized tomography and laparoscopic radioisotope guided sentinel lymph node dissection. J Urol 2006;176:2014–8.
[40] Wawroschek F, Vogt H, Weckermann D, Wagner T, Hamm M, Harzmann R. Radioisotope guided pelvic lymph node dissection for prostate cancer. J Urol 2001;166:1715–9.
[41] Brouwer OR, Buckle T, Vermeeren L, et al. Comparing the hybrid fluorescent-radioactive tracer indocyanine green-99mTc- nanocolloid with 99mTc-nanocolloid for sentinel node identification: a validation study using lymphoscintigraphy and SPECT/CT. J Nucl Med 2012;53:1034–40.
[42] Warncke SH, Mattei A, Fuechsel FG, Z'Brun S, Krause T, Studer UE. Detection rate and operating time required for gamma probe-guided sentinel lymph node resection after injection of technetium-99m nanocolloid into the prostate with and without preoperative imaging. Eur Urol 2007;52:126–33.
[43] van den Berg NS, Valdés-Olmos RA, van der Poel HG, van Leeuwen FW. Sentinel lymph node biopsy for prostate cancer: a hybrid approach. J Nucl Med 2013;54:493–6.
[44] Gupta AD, Han M. Imaging guidance in minimally invasive prostatectomy. Urol Oncol 2011;29:343–6.
[45] Moul JW, Kane CJ, Malkowicz SB. The role of imaging studies and molecular markers for selecting candidates for radical prostatectomy. Urol Clin North Am 2001;28:459–72.
[46] Ukimura O, Magi-Galluzzi C, Gill IS. Real-time transrectal ultrasound guidance during laparoscopic radical prostatectomy: impact on surgical margins. J Urol 2006;175:1304–10.
[47] van der Poel HG, de Blok W, Bex A, Meinhardt W, Horenblas S. Perioperative transrectal ultrasonography-guided bladder neck dissection eases the learning of robot-assisted laparoscopic prostatectomy. BJU Int 2008;102:849–52.
[48] Simpfendörfer T, Baumhauer M, Müller M. Augmented reality visualization during laparoscopic radical prostatectomy. J Endourol 2011;25:1841–5.
[49] Teber D, Simpfendörfer T, Guven S, Baumhauer M, Gözen AS, Rassweiler J. In-vitro evaluation of a soft-tissue navigation system for laparoscopic prostatectomy. J Endourol 2010;24:1487–91.
[50] Davila HH, Mamcarz M, Nadelhaft I, Salup R, Lockhart J, Carrion RE. Visualization of the neurovascular bundles and major pelvic ganglion with fluorescent tracers after penile injection in the rat. BJU Int 2007;101:1048–51.
[51] Natarajan S, Marks LS, Margolis DJ, et al. Clinical application of a 3D ultrasound-guided prostate biopsy system. Urol Oncol 2011;29:334–42.
[52] Adam C, Salomon G, Walther S, et al. Photodynamic diagnosis using 5-aminolevulinic acid for the detection of positive surgical margins during radical prostatectomy in patients with carcinoma of the prostate: a multicentre, prospective, phase 2 trial of a diagnostic procedure. Eur Urol 2009;55:1281–8.
[53] Yamaguchi T, Lee J, Uemura H, et al. Prostate cancer: a comparative study of (11)C-choline PET and MR imaging combined with proton MR spectroscopy. Eur J Nucl Med Mol Imaging 2005;32:742–8.
[54] Kotzerke J, Volkmer BG, Glatting G, et al. Intraindividual comparison of [11C]acetate and [11C]choline PET for detection of metastases of prostate cancer. Nuklearmedizin 2003;42:25–30.
[55] Cimitan M, Bortolus R, Morassut S, et al. [(18)F]fluorocholine PET/CT imaging for the detection of recurrent prostate cancer at PSA relapse: experience in 100 consecutive patients. Eur J Nucl Med Mol Imaging 2006;33:1387–98.
[56] Springer C, Hoda MR, Mohammed N, Fajkovic H, Fornara P, Greco F. Laparoscopic vs open partial nephrectomy for T1 renal tumors: evaluation of the long-term oncologic and functional outcomes in 340 patients. BJU Int 2013;111:281–8.
[57] Ukimura O, Gill IS. Imaging-assisted endoscopic surgery: Cleveland Clinic experience. J Endourol 2008;22:803–10.
[58] Tobis S, Knopf JK, Silvers CR, et al. Near infrared fluorescence imaging after intravenous indocyanine green: initial clinical experience with open partial nephrectomy for renal cortical tumors. Urology 2012;79:958–64.
[59] Tobis S, Knopf J, Silvers C, et al. Near infrared fluorescence imaging with robotic assisted laparoscopic partial nephrectomy: initial clinical experience for renal cortical tumors. J Urol 2011;186:47–52.
[60] Su LM, Vagvolgyi BP, Agarwal R, Reiley CE, Taylor RH, Hager GD. Augmented reality during robot-assisted laparoscopic partial nephrectomy: toward real-time 3D-CT to stereoscopic video registration. Urology 2009;73:896–900.
[61] Hoda MR, Popken G. Surgical outcomes of fluorescence-guided laparoscopic partial nephrectomy using 5-aminolevulinic acid-induced protoporphyrin IX. J Surg Res 2009;154:220–5.
[62] Wessels JT, Busse AC, Rave-Fränk M, et al. Photosensitizing and radiosensitizing effects of hypericin on human renal carcinoma cells in vitro. Photochem Photobiol 2008;84:228–35.

[63] Best SL, Thapa A, Holzer MJ, et al. Minimal arterial in-flow protects renal oxygenation and function during porcine partial nephrectomy: confirmation by hyperspectral imaging. Urology 2011;78:961–6.
[64] Olweny EO, Faddegon S, Best SL, et al. Renal oxygenation during robotic-assisted laparoscopic partial nephrectomy; characterization using laparoscopic digital light processing (DLP®) hyperspectral imaging. J Endourol 2013;27:265–9.
[65] Oguro S, Tuncali K, Elhawary H, Morrison PR, Hata N, Silverman SG. Image registration of pre-procedural MRI and intra-procedural CT images to aid CT-guided percutaneous cryoablation of renal tumors. Int J Comput Assist Radiol Surg 2011;6:111–7.
[66] Kang DE, White Jr RL, Zuger JH, Sasser HC, Teigland CM. Clinical use of fluorodeoxyglucose F 18 positron emission tomography for detection of renal cell carcinoma. J Urol 2004;171:1806–9.
[67] Ohyama C, Chiba Y, Yamazaki T, Endoh M, Hoshi S, Arai Y. Lymphatic mapping and gamma probe guided laparoscopic biopsy of sentinel lymph node in patients with clinical stage I testicular tumor. J Urol 2002;168:1390–5.
[68] Penna FJ, Freilich DA, Alvarenga C, Nguyen HT. Improving lymph node yield in retroperitoneal lymph node dissection using fluorescent molecular imaging: a novel method of localizing lymph nodes in Guinea pig model. Urology 2011;78, 232.e15–8.
[69] Lassen U, Daugaard G, Eigtved A, Hojgaard L, Damgaard K, Rorth M. Whole-body FDG-PET in patients with stage I non-seminomatous germ cell tumours. Eur J Nucl Med Mol Imaging 2003;30:396–402.
[70] Brouwer OR, Valdés-Olmos RA, Vermeeren L, Hoefnagel CA, Nieweg OE, Horenblas S. SPECT/CT and a portable gamma-camera for image-guided laparoscopic sentinel node biopsy in testicular cancer. J Nucl Med 2011;52:551–4.
[71] Cauberg ECC, de Bruin DM, Faber DJ, van Leeuwen TG, de la Rosette JJMCH, de Reijke TM. A new generation of optical diagnostics for bladder cancer: technology, diagnostic accuracy, and future applications. Eur Urol 2009;56:287–97.
[72] De Jong BW, Bakker Schut TC, Wolffenbuttel KP, Nijman JM, Kok DJ, Puppels GJ. Identification of bladder wall layers by Raman spectroscopy. J Urol 2002;168:1771–8.
[73] Kausch I, Sommerauer M, Montorsi F, et al. Photodynamic diagnosis in non–muscle-invasive bladder cancer: a systematic review and cumulative analysis of prospective studies. Eur Urol 2010;57:595–606.
[74] Jocham D, Stepp H, Waidelich R. Photodynamic diagnosis in urology: state-of-the-art. Eur Urol 2008;53:1138–50.
[75] Hermann GG, Mogensen K, Carlsson S, Marcussen N, Duun S. Fluorescence-guided transurethral resection of bladder tumours reduces bladder tumour recurrence due to less residual tumour tissue in Ta/T1 patients: a randomized two-centre study. BJU Int 2011;108:297–303.
[76] Grossman HB, Stenzl A, Fradet Y, et al. Long-term decrease in bladder cancer recurrence with hexaminolevulinate enabled fluorescence cystoscopy. J Urol 2012;188:58–62.
[77] Herr HW, Donat SM. A comparison of white-light cystoscopy and narrow-band imaging cystoscopy to detect bladder tumour recurrences. BJU Int 2008;102:1111–4.
[78] Geavlete B, Jecu M, Multescu R, Geavlete P. Narrow-band imaging cystoscopy in non-muscle-invasive bladder cancer: a prospective comparison to the standard approach. Ther Adv Urol 2012;4:211–7.
[79] Naselli A, Introini C, Timossi L, et al. A randomized prospective trial to assess the impact of transurethral resection in narrow band imaging modality on non–muscle-invasive bladder cancer recurrence. Eur Urol 2012;61:908–13.
[80] Drieskens O, Oyen R, Van Poppel H, Vankan Y, Flamen P, Mortelmans L. FDG-PET for preoperative staging of bladder cancer. Eur J Nucl Med Mol Imaging 2005;32:1412–7.
[81] Kuehhas FE, Weibl P, Tosev G, Schatzl G, Heinz-Peer G. Multidetector computed tomography virtual cystoscopy: an effective diagnostic tool in patients with hematuria. Urology 2012;79:270–6.
[82] Qu X, Huang X, Wu L, Huang G, Ping X, Yan W. Comparison of virtual cystoscopy and ultrasonography for bladder cancer detection: a meta-analysis. Eur J Radiol 2011;80:188–97.
[83] Salomon G, Spethmann J, Beckmann A, et al. Accuracy of HistoScanning™ for the prediction of a negative surgical margin in patients undergoing radical prostatectomy. BJU Int 2013;111:60–6.
[84] Finley DS, Ellingson BM, Natarajan S. Diffusion tensor magnetic resonance tractography of the prostate: feasibility for mapping periprostatic fibers. Urology 2012;80:219–23.